Quaternary Research 75 (2011) 721–733

Contents lists available at ScienceDirect

Quaternary Research

journal homepage: www.elsevier.com/locate/yqres

Regional mapping and characterisation of old landslides in hilly regions using LiDAR-based imagery in Southern Flanders

M. Van Den Eeckhaut [a,b,*], Jean Poesen [b], Frans Gullentops [b], Liesbeth Vandekerckhove [c], Javier Hervás [a]

[a] Land Management and Natural Hazards Unit, Institute for Environment and Sustainability, Joint Research Centre (JRC)–European Commission, 21027 Ispra (VA), Italy
[b] Division of Geography, Department of Earth and Environmental Sciences, K.U.Leuven, Celestijnenlaan 200E, B-3001 Heverlee, Belgium
[c] Environment, Nature and Energy Department, Flemish Government, Brussels, Belgium

ARTICLE INFO

Article history:
Received 29 April 2010
Available online 10 March 2011

Keywords:
Quaternary landslides
LiDAR-derived shaded-relief maps
Deep-seated gravitational slope deformation
Topographical threshold
Frequency–size distribution
Seismic trigger

ABSTRACT

Analysis of LiDAR-derived imagery led to the discovery of more than 330 pre-Holocene to recent landslides in Southern Flanders (4850 km^2). The morphology of three landslides, including the 266.5 ha deep-seated gravitational slope deformation in Alden Biesen, was investigated in more detail. The analysis of the morphological and topographical characteristics (width–length relation, frequency–area distribution and topographical threshold) of the landslides revealed important differences compared to the characteristics reported in other landslide studies, and helped understanding possible landslide triggering mechanisms. Especially the possibility of a seismic origin of the landslides was investigated. Finally, a heuristic model for region-wide landslide susceptibility mapping was successfully tested. The susceptibility model and map allow prediction of future landslide locations and contribute to better understanding the role of individual causal factors on landslide location and spatial density. The results suggest that landslides on low-gradient, soil-mantled hills are a more important contributor to landscape evolution of hilly areas than was hitherto thought. The morphology of all hilly regions of Flanders is clearly marked by landslide processes and higher landslide densities often coincide with the presence of quaternary active faults. This study further shows that high-resolution topographical data such as LiDAR significantly contributes to a better detection of old, previously unknown landslides.

Introduction

The wide range of light detection and ranging (LiDAR) derivative products has recently become a powerful tool in landslide research, particularly for landslide identification and landslide inventory mapping. Although already used in landslide studies for decades, shaded-relief, slope, surface roughness and contour maps (Ardizzone et al., 2007; Schulz, 2007; Haneberg et al., 2009) have regained popularity since the availability of LiDAR. Being derived from LiDAR these surface maps allow more accurate and complete landslide mapping compared to those that are, for example, derived from contours on the topographical map (Van Den Eeckhaut et al., 2005, 2007a). In forested areas LiDAR derivatives have also proven more useful compared to traditional passive optical imagery (Haugerud et al., 2003; Rowlands et al., 2003; Haneberg, 2005).

In contrast to the many studies that use expert-based analysis of LiDAR derivatives to identify landslides, only few studies have attempted to develop computer-aided methods for extracting landslides from LiDAR data (McKean and Roering, 2004; Glenn et al., 2006; Booth et al., 2009). Promising results were obtained with surface roughness parameters (Glenn et al., 2006; Kasai et al., 2009), but regional-scale automatic landslide extraction from LiDAR derivatives remains difficult.

So far, all LiDAR-derived landslide inventories also cover rather limited areas. The study areas of Tarolli and Tarboton (2006), Haneberg et al. (2009) and Kasai et al. (2009) were at most 10 km^2. Somewhat larger study areas were investigated by Ardizzone et al. (2007) (90 km^2), Van Den Eeckhaut et al. (2007a) (125 km^2), Booth et al. (2009) (176 and 212 km^2) and Schulz (2007) (215 km^2). We, however, focus on a 4850 km^2 area in Southern Flanders in this study, and use LiDAR-derived images to investigate pre-Holocene to recent landslides and their spatial impact on the local morphology. The specific goals of the study are to: (1) identify the landslides and produce a landslide inventory map of the study area; (2) analyse the morphological and topographical characteristics of the mapped landslides; (3) test a procedure for the efficient production of region-wide landslide susceptibility maps; and (4) use the topographical threshold and frequency–size distribution to formulate hypotheses on the genesis of the landslides. Important differences with previous landslide studies using LiDAR for landslide identification are the size of the selected study area (4850 km^2) and the direct implementation of the obtained landslide inventory for testing a heuristic model for

* Corresponding author at: Land Management and Natural Hazards Unit, Institute for Environment and Sustainability, Joint Research Centre (JRC)–European Commission, 21027 Ispra (VA), Italy.
E-mail address: miet.van-den-eeckhaut@jrc.ec.europa.eu (M. Van Den Eeckhaut).

0033-5894/$ – see front matter © 2011 University of Washington. Published by Elsevier Inc. All rights reserved.
doi:10.1016/j.yqres.2011.02.006

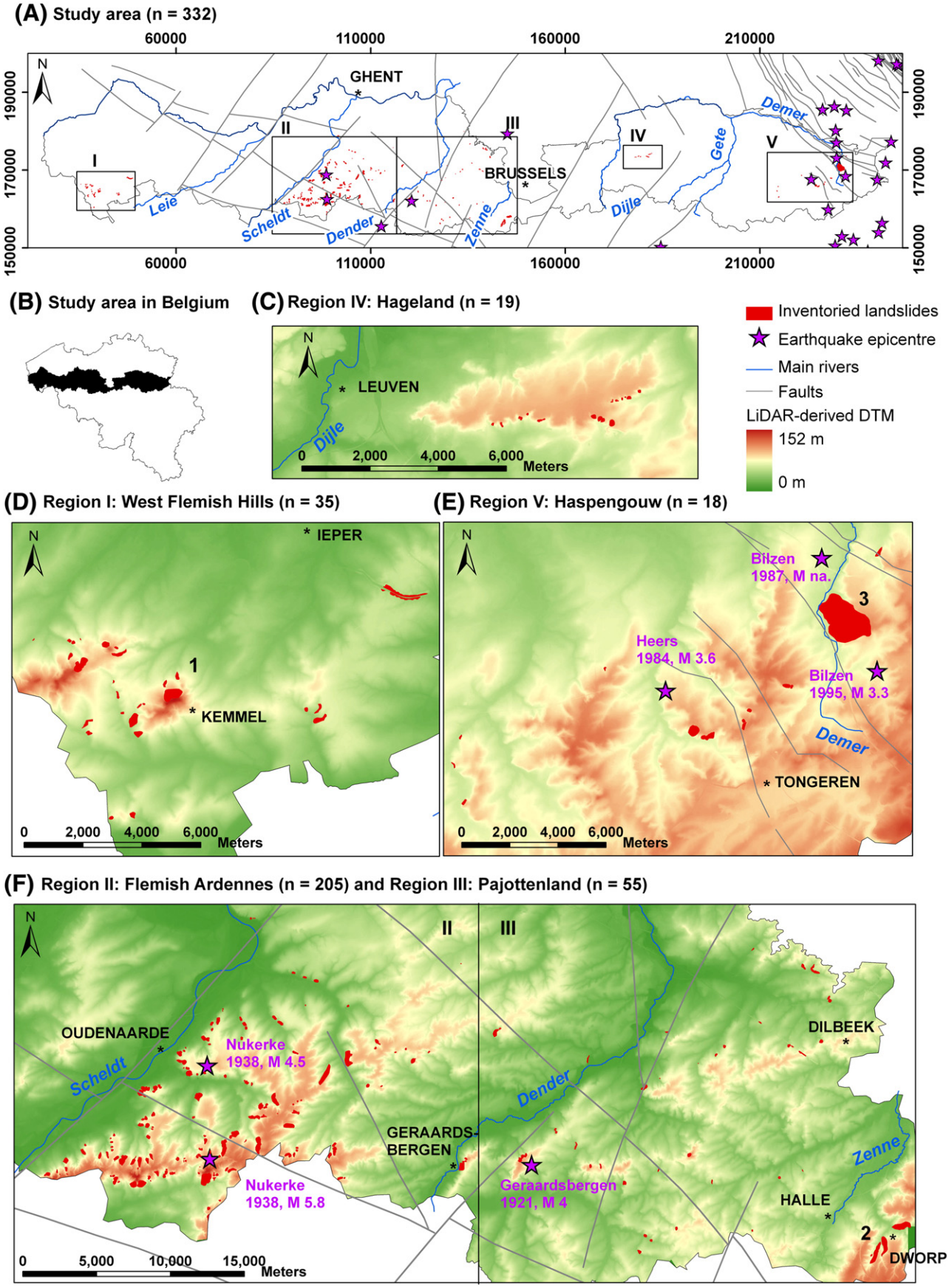

Figure 1. Study area: (A) regions in Southern Flanders where landslides were detected and mapped (Belgian Lambert 72 coordinates; m); (B) study area in Belgium; (C) landslides in Hageland; (D) landslides in West Flemish hills; (E) landslides in Haspengouw; (F) landslides in Flemish Ardennes and Pajottenland. DEM excerpts are derived from LiDAR and numbers 1 to 3 show the location of the Kemmelberg landslide (1), the Hallerbos landslide (2) and the Alden Biesen landslide (3).

landslide susceptibility mapping at the regional scale (i.e. 1:10,000 to 1:50,000).

Study area

The topography of Flanders (Northern Belgium) can be broadly divided into two zones (Fig. 1A): Northern Flanders, where slopes are generally too low for natural landslides to occur; and Southern Flanders, the focus of this study, where slopes are often steeper than 5%. The 4850 km^2 area of Southern Flanders contains five hilly regions underlain by Tertiary rock (Fig. 1A). From west to east these are the West Flemish hills (up to 155 m above sea level; a.s.l.), the hills of the Flemish Ardennes (up to 156 m a.s.l.), the Pajottenland hills (up to 112 m a.s.l.), the Hageland hills (up to 105 m a.s.l.) and the Haspengouw hills (up to 128 m a.s.l.). These hilly regions are separated by wide valleys of the Leie, Scheldt, Dender, Dijle and Gete rivers. Landslides have been previously reported only in the Flemish Ardennes (Halet, 1904; Lefèvre, 1926–1927; Vanmaercke-Gottigny, 1980; Ost et al., 2003; Van Den Eeckhaut et al., 2005, 2007a; Dewitte et al., 2006).

In Flanders, the lithology consists primarily of unconsolidated Late Miocene to Early Palaeocene Tertiary sediments with some west–east variability in the distribution of stratigraphic units (Table 1). The Tertiary formations consist of subhorizontal layers of alternating sand, clay and clay-silt gently dipping at 0.4% towards the northeast (Jacobs et al., 1999). Quaternary seismicity in Southern Flanders is influenced by two fault zones (Fig. 1A): the Nieuwpoort-Asquempont Fault Zone crosses almost the complete study area, and the faults related to the Roer Graben along the Lower Rhine Embayment located east of the study area. The Nieuwpoort-Asquempont Fault Zone contains west–east-trending longitudinal faults and southwest–northeast-trending transverse faults (Chacksfield et al., 1993; De Vos et al., 1993). Fault activity probably started in the Silurian (Debacker et al., 2004). At present the complete fault zone is still seismically active, but especially the longitudinal faults are able to cause earthquakes with a magnitude up to 6 (Camelbeeck, 1997). During the last 100 years, two earthquakes with epicentres in the study area occurred, in 1921 (Geraardsbergen; magnitude, $M=4$) and 1938 (Nukerke; $M=5.8$; Fig. 1F). Although Somville (1939) reported that the 1938 earthquake had an important impact on the groundwater flow as new springs were formed and existing springs were relocated, no historical document linking landslide activity to earthquakes has been found. For the eastern fault zone, related to the northwest-southeast-oriented Roer Graben, indications are found that during the last 30 ka at least three earthquakes with M between 6.2 and 6.8 and return period ranging from 10 to 20 ka occurred (Camelbeeck et al., 2000). Earthquakes with lower magnitudes occur more frequently (e.g. Fig. 1A and E). The last large earthquake felt in the study area was the M 5.8 Roermond earthquake of 1992.

Materials and methods

LiDAR-derived landslide inventory

The LiDAR data (AGIV, 2005) used in this study are similar to the data used for a smaller study area by Van Den Eeckhaut et al. (2007a). Flights took place in 2001 and 2002. An Azimuth Aeroscan small footprint (30 cm) multi-return LiDAR system with a pulse rate of

Table 1
Lithostratigraphical table of Southern Flanders showing presence (indicated by +) of the geological formations west and east of Brussels. Clay-rich deposits susceptible to landslide initiation are in bold (derived from Jacobs et al., 1999; Claes et al., 2001).

Chronostratigraphy (10^6 years)		Lithostratigraphy		Lithology	West of Brussels	East of Brussels
		Formation	Member*			
Tertiary	Miocene (23.8–5.4)	Diest		Sand	+	+
		Bolderberg		Sand		+
	Oligocene (33.6–23.8)	Eigenbilzen		Sand		+
		Boom		Clay		+
		Bilzen		Sand with clay layer in between		+
		Borgloon	Alden Biesen	Sand		+
			Henis	**Clay**		+
		Sint-Huibrechts Hern		Sand		+
	Eocene (54.8–33.6)	Maldegem	Onderdijke	Clay	+	
			Buisputten	Sand	+	
			Zomergem	Clay	+	
			Onderdale	Sand	+	
			Ursel	**Clay**	+	
			Asse	**Clay**	+	
			Wemmel	Sand	+	
		Lede		Sand	+	
		Brussel		Sand		+
		Aalter		Sand	+	
		Gent	Vlierzele	Sand with clay lenses	+	
			Pittem	**Clay**	+	
			Merelbeke	**Clay**	+	
		Tielt		Clayey sand alternated with **clay layers**	+	
		Kortrijk	**Aalbeke**	**Clay**	+	+**
			Moen	Clayey silt and sand alternated with **clay layers**	+	
			St.-Maur	Silty clay	+	
			Mont-Héribu	Clayey sand or sandy clay	+	
	Paleocene (65–54.8)	Tienen		Sand		+
		Hannut		Sand	+	+
		Heers		**Marl**		+
		Houthem		Limestone		
	Cretaceous (83.5–65)	Maastricht		Calcarenite		+
		Gulpen		Chalk		+

* Only members relevant for this landslide study are mentioned.
** East of Brussels this clayey formation is not subdivided in different members.

15 kHz and vertical accuracy (RMSE) of 4 cm was used. Laser pulses were sent at equal intervals within 600 m wide swaths with average pulse density of 1 per 4 m^2. The last return from each pulse was assumed to be from the soil surface, although this was not always the case. Terrascan software was used by the vendor for the production of the bare earth DTM, and a manual check followed. The data have a point density of at least 1 per 20 m^2, a horizontal accuracy below 15 cm and an average vertical accuracy that depends on vegetation height, decreasing from 7 cm for freshly cut lawn to 20 cm for pastures and forests (GIS-Vlaanderen, 2003). Although the pulse density and spatial accuracy of LiDAR systems have improved since 2002, the acquisition of new, more detailed LiDAR data was not required, as the data are of sufficient detail for landslide identification (Van Den Eeckhaut et al., 2007a) and no major landslide triggering events occurred since 2002.

From the LiDAR point data, a Triangulated Irregular Network (TIN) was derived. The TIN was then converted to a DTM with a 2 m resolution, and shaded-relief maps and a contour map (2 m interval) were created. After comparing shaded-relief maps with different sun elevation and sun azimuth angles and without vertical exaggeration, those with a sun elevation angle of 30° and a sun azimuth angle of 315° and 45° were selected for further analysis because landslides were most easily identifiable on these two maps.

Landslide identification on shaded-relief and contour maps is based on the recognition of landslide features (e.g. main scarps, stair-stepped patterns of displaced backward-rotated blocks, also called reverse slopes, and convex landslide toes) and alterations of the drainage system (e.g. a main valley stream pushed away by a landslide). Between two and four geomorphologists were asked to digitize the 'presumed' landslides on a vector map which could be overlain on the shaded-relief and contour line maps. Presumed landslides were digitized as closed polygons including the whole affected area from the main scarp to the landslide toe, generally at scales between 1:4000 and 1:10,000. Then, presumed landslide sites were compared with orthophotos to exclude sites with anthropogenic disturbance incorrectly classified as possible landslides (e.g. quarries, construction sites). All the remaining sites ($n \approx 450$) and surrounding hillslopes ($n \approx 150$) were checked in the field by one or two geomorphologists in order to produce the final landslide inventory. Surrounding hillslopes located close to mapped landslides were mainly checked for the presence of relatively small landslides (landslide-affected area, $A_L < 1.0$ ha), which are more difficult to identify from LiDAR derivatives. Recent landslides were further tracked by checking newspapers and technical reports and by placing advertisements in local newspapers. The produced landslide inventory is thus a historical inventory containing landslides of different ages and triggering events. In the field, all landslides were classified according to Cruden and Varnes (1996). Based on the depth of the surface of rupture, which was estimated in the field, landslides with a surface of rupture deeper than 3 m, but generally deeper than 10 m, and landslides with a surface of rupture at a depth of less than 3 m were classified deep-seated and shallow, respectively. For estimating the volume displaced by the landslides (V, m^3) the formula for landslides with a curved surface of rupture as proposed by Cruden and Varnes (1996) was adopted:

$$V = \frac{1}{6} \cdot \pi \cdot D \cdot W \cdot L \quad (1)$$

with D the depth of the surface of rupture (m), W the width of the surface of rupture (m), and L the landslide length (m).

Frequency–size distribution

The frequency–size distribution $f(A_L)$ of one or more landslide events quantifies the number of landslides of different sizes (Malamud et al., 2004). For landslide inventories many $f(A_L)$ scaling is characterised by two scaling regimes, often described by a Double Pareto probability function (Stark and Hovius, 2001; Guthrie and Evans, 2004) or a three-parameter inverse-gamma probability distribution (Malamud et al., 2004; Korup and Clague, 2009). More specifically the two scaling regimes show a negative power–law scaling for medium-size and large landslides, and a positive power–law scaling for small landslides. The inflection point between the two power–law relations is termed rollover. Historical inventories, such as the one of Southern Flanders, are assumed to be incomplete as morphological characteristics of old shallow landslides can be obliterated by human activities and soil erosion or hidden by dense vegetation. Therefore, historical inventories are thought to have a $f(A_L)$ with the same two scaling regimes, but with a shift of the rollover towards larger areas (Malamud et al., 2004). Only few studies have questioned the universality of the power–law landslide area distributions and presented area or volume distributions that were logarithmic (Issler et al., 2005) or lognormal (Dunning et al., 2007; ten Brink et al., 2009). Van Den Eeckhaut et al. (2007b) obtained a size-distribution consisting of two separate negative power–law relations for small and medium-sized to large landslides in the Flemish Ardennes. Only the distribution of the medium-size to large, deep-seated landslides was in agreement with common findings. An explanation for the different distribution of the small landslides is that these were mainly triggered by local human activities. Such human activities typically decrease the slope stability only locally so that the number of human-induced landslides decreases with landslide size and a negative power–law function is obtained (see conceptual model (Fig. 5) in Van Den Eeckhaut et al., 2007b).

Topographical threshold

Landslides become more frequent above a threshold slope gradient and preferentially initiate in areas of topographic convergence where subsurface flow concentrates (Siddle et al., 1985). Therefore, the relationship between slope gradient (S, %) and drainage area (A, ha), often used as a surrogate measure of surface and subsurface flow accumulation in topographic convergence, has been investigated for initiation of landslides (e.g. Montgomery and Dietrich, 1994a,b; Moeyersons et al., 2004). Similarly S-A thresholds have been defined for other soil erosion processes such as soil piping (e.g. Verachtert et al., 2010) and gullies (e.g. Poesen et al. 2003; Vanwalleghem et al., 2005). The relation is generally described using a negative power–law relationship:

$$S = a A^{-b} \quad (2)$$

with a a constant (−) and b the area exponent (−), both depending on environmental characteristics. The topographical threshold is defined as the line drawn through the lowermost observations in the S-A space parallel to the power–law regression.

In this study, S represents the mean slope of a landslide, calculated for all deep-seated landslides from a LiDAR-derived contour map with 2 m intervals by dividing the elevation difference between the highest and lowest point on the landslide by the distance between these two points. A represents the drainage area of the main scarp and was calculated with the spatially distributed soil erosion and sediment delivery model, WaTEM/SEDEM (Verstraeten et al., 2002), using a 20 m DTM. Since A is estimated from the surface topography and the initiation of landslides is mainly depending on subsurface flow, we have to assume that the surface and subsurface A have the same size. As the lithological stratification in Southern Flanders is subhorizontal, this assumption is correct. Furthermore, anthropogenic structures (roads, drainage ditches, etc.) influence the true size of A (Montgomery, 1994), but as in most studies they are not taken into account in the estimated A.

Table 2
Classification scheme used for the production of the heuristic landslide susceptibility map, and proportion of the study area and the mapped landslides within the different classes.

Susceptibility		Variables		Study area		Landslides	
	Class*	Lithology	Slope (S; %)	%	Cumulative	%	Cumulative
High	VI	Clay	S≥15	0.9	0.9	31.3	31.3
	V	Clay	10≤S<15	2.2	3.1	28.0	59.2
	IV	Clay	8≤S<10	0.8	4.0**	4.2	63.5***
Low	III	Clay	6≤S<8	3.7	7.6	9.0	72.5
	II	Clay	S<6	61.4	69.0	9.5	82.0
	I	Sand		31.0	100.0	18.0	100.0

* Susceptibility classes ($n=6$) of the intermediate landslide susceptibility map. The final susceptibility map has only two classes, high and low landslide susceptibility.
** Percentage of the study area (i.e. Southern Flanders; i.e. 4850 km^2) classified as highly susceptible by the model.
*** Percentage of mapped landslides located within highly susceptible areas.

Landslide susceptibility

A landslide susceptibility map shows the spatial distribution of the actual and potential landslides while a landslide risk map contains information on the expected number of lives lost, persons injured, damage to properties, or disruption of economic activity due to a particular landslide (Van Westen, 1993). Given that for the landslides in Southern Flanders information on the initiation date is only available for a few landslides reported in the last 50 years and that no information on damage is available, only a susceptibility map can be produced. A review of landslide susceptibility modelling literature indicated that topography and lithology are the most frequently used and most important controlling factors (Ercanoğlu, 2003). Also in the Flemish Ardennes, slope and lithology are the controlling factors with the highest predictive power (Dewitte et al., 2006; Van Den Eeckhaut et al., 2006). Therefore, this study tested a heuristic landslide susceptibility model based on slope gradient and lithology only. Given that for large landslides, characteristics of depletion (initiation) and accumulation areas are significantly different, we mainly focus on prediction of landslide initiation areas. The scoring and classification matrix is based on slope gradient and lithology results from this and previous studies in Flanders. Van Den Eeckhaut et al. (2006) found that landslides in the Flemish Ardennes mainly occur on hillslopes with gradients of 10% or steeper and with clay lithology. Thus the 10 m × 10 m slope map was divided in five classes (i.e. slope<6%; 6%≤slope<8%; 8%≤slope<10%; 10%≤slope<15%; slope≥15%) and the geological map (10 m×10 m; AGIV, 2001) was reclassified in two classes, the first consisting of sandy layers and the second of clays and marls. The slope and lithology classifications were then combined to produce an intermediate landslide susceptibility map consisting of six classes (Table 2). The distribution of the landslides over the six classes was used as an indication of the prediction accuracy, and finally, a more general susceptibility map with two classes (high and low) was produced.

Results

Landslide inventory

The landslide inventory map shows the location of 332 landslides with a non-uniform distribution across Southern Flanders (Fig. 1A). The majority of the landslides were observed in the Flemish Ardennes ($n=205$; Fig. 1F), followed by Pajottenland ($n=55$; Fig. 1F), West Flemish hills ($n=35$; Fig. 1D), Hageland ($n=19$; Fig. 1C) and Haspengouw ($n=18$; Fig. 1E). Deep-seated rotational earth slides dominate, accounting for 65% ($n=217$; Table 3) of the mapped landslides. Seven percent ($n=23$) of the deep-seated landslides were classified as complex landslides. Two landslides in Haspengouw are characterised by a large earth mass that was detached as one block from the plateau, forming an isolated hill. The downslope movement of the large earth mass displaced the uppermost several meters of soil downslope from it, forming a convex landslide foot. These two landslides were classified as deep-seated gravitational slope deformations (DGSDs), phenomena that are defined to affect an entire slope and to be generated by mechanical processes such as deep-seated block sliding and lateral spreading (Moro et al., 2009). The Alden Biesen DGSD (nr. 3 in Fig. 1E) will be discussed in more detail in the next section. Twenty-seven percent ($n=90$) of all inventoried landslides are shallow complex landslides (Fig. 2B). For about 50 shallow landslides more detailed information of the initiation or reactivation date was found. With exception of four landslide events reported between AD 1828 and AD 1926, all the landslide events occurred after AD 1960. Although for the remaining shallow landslides no information on the timing was found, many of them showed signs of recent activity. The smallest landslides identified had a landslide affected area (A_L) of 0.5–0.75 ha.

There is a high degree of variability in the characteristics of landslides for each type (Table 3). For example, the mean A_L of a deep-seated rotational earth slide is 3.9 ha, but A_L varies from 0.2 to 40.4 ha.

Table 3
Morphological characteristics of the different landslide types mapped in Southern Flanders.

Type			Number	Affected area (A_L; ha)	Length (L; m)	Width (W; m)	Slope (S; %)*
Deep ≥3 m	Rotational	Mean	217	3.9	160	220	17
		Range		0.2–40.4	20–640	25–1450	6–67
	Complex	Mean	23	3.5	205	105	19
		Range		0.2–42.0	60–820	20–630	10–35
	DGSD**	Mean	2				
		Range		7–266.5	360–2200	240–1510	3–7
Shallow <3 m	Complex	Mean	90	0.60	70	70	18
		Range		0.007–3.15	10–200	8–250	8–40

* Slope is measured from the top of the main landslide scarp to the toe of the landslide.
** DGSD is deep-seated gravitational slope deformation.

Figure 2. Illustration of landslides in Southern Flanders. (A) Main scarp (left) and reverse slope (right) of a large, deep-seated rotational earth slide (Kemmelberg landslide, December 2008; see nr. 1 in Figs. 1D and 7). Persons indicate scale. (B) Frontal view on two adjacent shallow complex slides located in the West Flemish hills (Dranouter landslide, March 2009).

Deep-seated complex slides have a similar A_L range as the deep-seated rotational earth slides. All landslide types, except for the DGSDs, have mean slope gradients between about 17 and 19%. A last important characteristic of deep-seated rotational earth slides can be derived from Figure 3. A plot of landslide length versus landslide width shows that whereas deep-seated complex landslides are generally longer than wide, this is not the case for the deep-seated rotational slides. The Hallerbos landslide (nr. 2 in Fig. 1F; next section) illustrates the asymmetry between the length and width of the rotational slides in Southern Flanders.

Description of three representative or remarkable landslides

Here we provide detailed information on three old deep-seated landslides. Despite their large areas (18.4–266.5 ha) these landslides were only discovered during analysis of LiDAR data. Two of the deep-seated landslides, Alden Biesen and Kemmelberg, are at or adjacent to important archaeological and historical sites.

Alden Biesen DGSD

The Alden Biesen DGSD is located in the eastern part of Flanders near the town of Bilzen (nr. 3 in Fig. 1E). With an area of 266.5 ha, it is the largest landslide in Southern Flanders, being significantly larger than the second largest landslide in the region (i.e. 42.0 ha Muziekberg landslide in the Flemish Ardennes). Its estimated volume is 10×10^6 m^3 to 17×10^6 m^3. With the exception of the Kolmont landslide (7.0 ha) located less than 10 km southwest of Alden Biesen, no other DGSD was found in Southern Flanders.

The geomorphological map and the shaded-relief map of the landslide (Fig. 4) show a main scarp with a gentle slope gradient (12%). Downslope of the main scarp, there is first an isolated hill and then a convex landslide foot which displaced the Demer river probably more than 500 m, and within which two reverse slopes were identified. The topography of these reverse slopes is locally subdued due to soil tillage. Along both flanks of the main scarp, towards the Demer river a drainage network, typical for old landslides with a subdued morphology (Keaton and DeGraff, 1996; Mather et al., 2003), has developed. The current landslide morphology suggests that when the landslide initiated, a very large earth mass must have been detached from the plateau (currently at 110 m a.s.l.), probably by a combination of lateral spreading and rotational sliding. Displaced over a distance of about 450 m, this earth mass nowadays forms an isolated hill of 104 m a.s.l. in the landscape. Upon detachment of the earth mass, additional soil material moved downslope forming the convex landslide footslope and

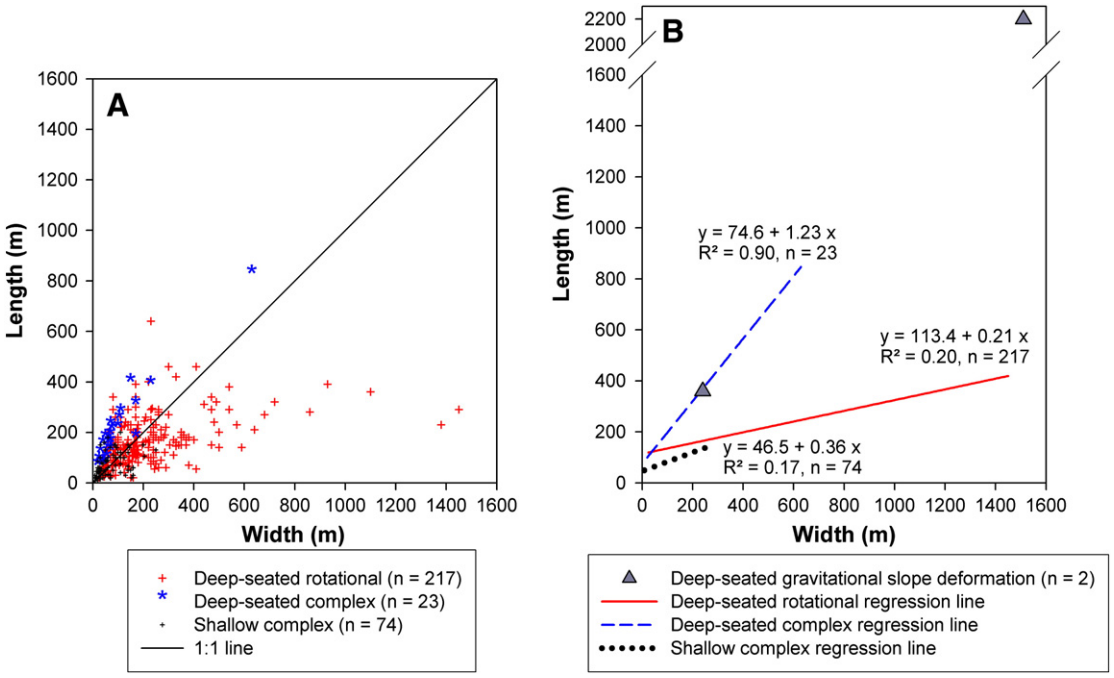

Figure 3. Length–width relation of deep-seated rotational, deep-seated complex and shallow complex landslides in Flanders.

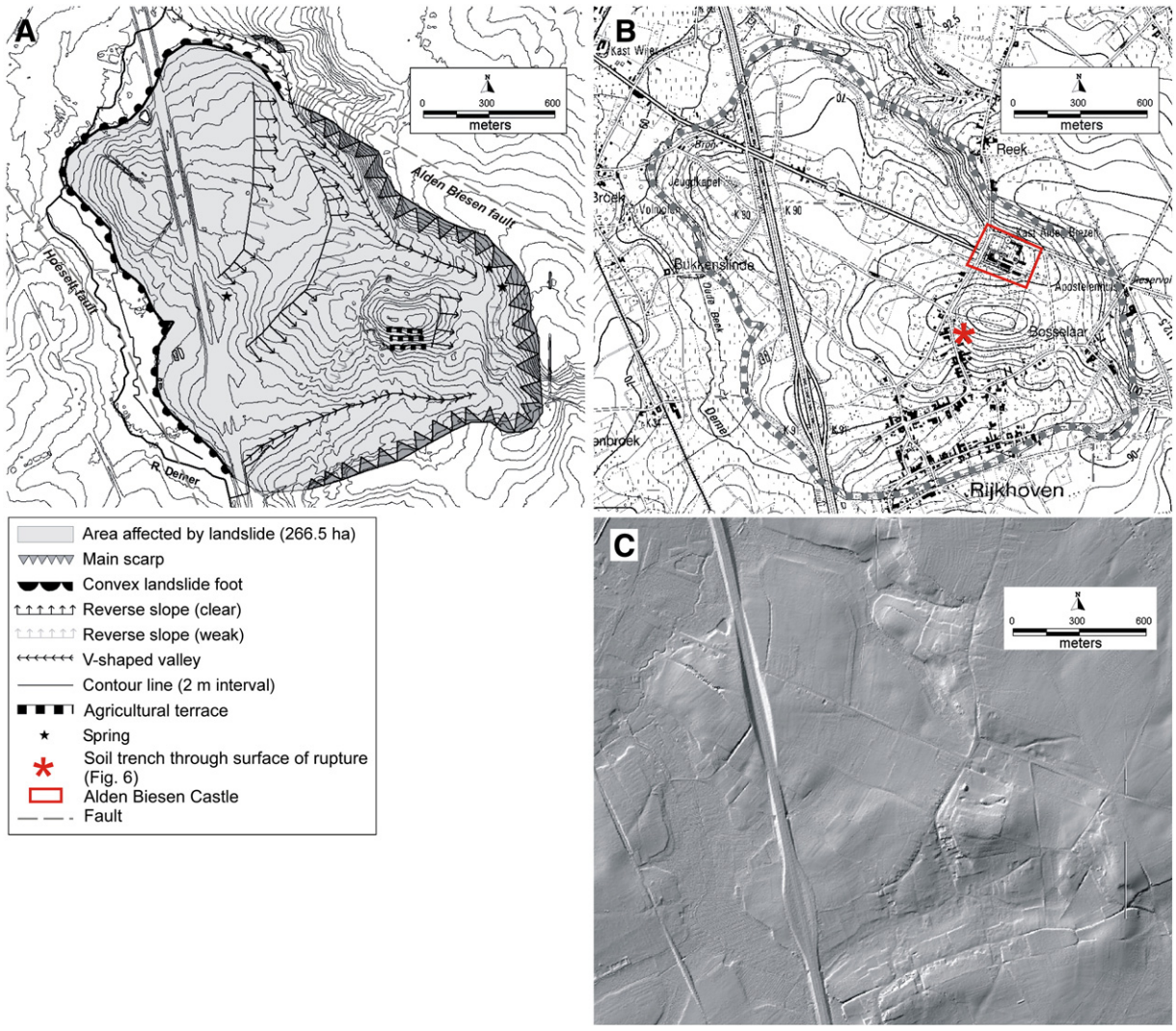

Figure 4. The Alden Biesen landslide near Bilzen, the largest deep-seated landslide mapped in Flanders ($A_L = 266.5$ ha; see nr. 3 in Fig. 1E). (A) Geomorphological map. (B) Excerpt of the topographical map. (C) Excerpt of the LiDAR-derived shaded-relief map.

displacing the Demer river. As the landslide foot has three distinct lobes, several activity phases might have occurred.

Close to the landslide there are several active WNW-ESE trending faults affecting the Cretaceous and Tertiary strata (Figs. 1 and 4; Gullentops and Claes, 1997; Claes et al., 2001). These faults are related to the Roer Graben and were active during the Quaternary. The northern flank of the landslide more or less coincides with the location of the Alden Biesen fault, while the Hoeselt fault runs parallel to the Demer river and borders the landslide foot. Information on local lithology (Dreesen et al., in press) suggests that the large earth mass has been sliding over and within the Henis Clay (Borgloon Formation; Table 1). This is in agreement with observations made in a trench excavated for construction of a building in the west-facing footslope of the isolated hill. This trench (Fig. 5) clearly reveals a surface of rupture with well-preserved overturned folds. The reverse slopes observed downslope of the isolated hill further suggest displacement over sliding planes in the sediment deposits below the Henis Clay (i.e. Sint-Huibrechts Hern Formation generally consisting of very fine sands), but a detailed study is needed to determine the lithological characteristics of these deposits.

Currently many buildings are located within the landslide (Fig. 4B). Important is the location of the Alden Biesen castle (16th-18th century) north of the isolated hill (Jenniskens, 1989). Although the deep-seated landslide is currently dormant or inactive, but with a high probability of local reactivation, at least 15–20 buildings, mainly houses, with large cracks were identified during a field survey. These buildings are between 20 and 100 years old and mainly located downslope of the isolated hill, indicating that this part of the landslide is most susceptible to local reactivation. Digging of the trench shown in Figure 5 in the summer of 2007 caused local landslide reactivation. Due to the removal of the lateral support, a large part of the trench wall collapsed in the weeks following the field visit.

Hallerbos landslide

The Hallerbos landslide is located southwest of Brussels, near the town of Dworp (nr. 2 in Fig. 1F). It is a rotational earth slide, currently under forest. Historical records of the Hallerbos forest date back to the 7th century (De Keersmaeker et al., 2007). Since then, it was probably never completely deforested. The absence of important human activity explains the fresh landslide characteristics. The geomorphological map and shaded-relief map (Fig. 6) show from east to west a clear main scarp (10 m high with a slope of 17%) and several well-preserved reverse slopes. Although rotational earth slides in the study area generally have width/length ratio's exceeding 1 (Fig. 3) the Hallerbos landslide is, with its width of 1380 m and length of 230 m, the landslide with the highest width/length ratio. Having an affected area of 21.1 ha and a displaced volume between 1.0×10^6 m^3 and 1.7×10^6 m^3, it is also one of the larger, deep-seated rotational earth

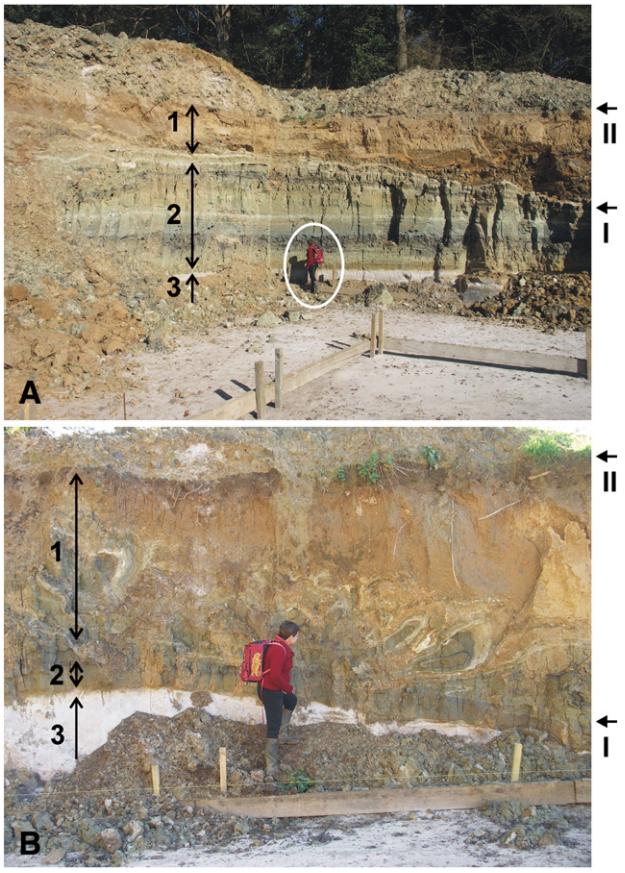

Figure 5. Trench through sliding plane of Alden Biesen landslide (October 2007; see nr. 3 in Figs. 1E and 4). (A) Overview of north-south oriented wall. (B) Detail of east–west oriented wall: surface of rupture with overturned folds. I: surface of rupture or sliding plane; II: soil surface; 1: displaced material (Henis clay and Quaternary loam); 2: Henis clay; 3: paleosoil in Sint-Huibrechts Hern sands.

slides. In contrast to most deep-seated landslides west of Brussels, the surface of rupture of the Hallerbos landslide is not located in the homogeneous smectite-rich (>50%) clays of the Aalbeke Member (Kortrijk Formation; Table 1), but in the silty clays of the older Moen or St-Maur Member. Buffel and Matthijs (2009) found strong indications for the presence of six NNE-SSW oriented faults 7–20 km east of the landslide. Discontinuities in the lithology indicate that this fault system was active during the Middle and Late Eocene and were linked to activity of the Nieuwpoort-Asquempont Fault Zone of which a major fault is located less than 8 km south of the landslide.

Kemmelberg landslide

The Kemmelberg landslide, located near the town of Kemmel in the western part of the study area, is a deep-seated rotational earth slide that affects the whole northern flank of the Kemmelberg hill (nr. 1; Fig. 1D). This 156 m high hill is mainly known as a strategic observation point during World War I. The French ossuary and statue remember to this period. The Kemmelberg hill is also an important archaeological site, because on the plateau and on the northern flank of this hill remnants of a Celtic site were found (Van Doorselaer et al., 1987). Apart from landsliding, bombing and digging of trenches during the war and archaeological excavations, also local extraction of Diestian sandstone have influenced the hill's local topography. Hence, only after collecting detailed information on anthropogenic changes in local topography (e.g. local irregular morphology related to archaeological excavations downslope of the main scarp) from archaeologists and historians specialized in World War I, a geomorphological interpretation of the site was made. The geomorphological map and shaded-relief map (Fig. 7) suggest that the landslide had at least three distinct activity phases because the main scarp consists of three semi-circular scarps and the landslide foot shows different convex lobes. In total an area of 18.4 ha, and a volume between 0.4×10^6 $m^3$and 0.8×10^6 m^3 was affected. Similar to the Alden Biesen landslide, a drainage system has developed along the flanks, evacuating water exfiltrating from springs at the bottom of the main scarp. Downslope of the main scarp up to three reverse slopes were found (Figs. 2A and 7), with water ponding in at least two of them. On the eastern lobe of the landslide foot, the Flemish Water Company constructed about 40 years ago a building, showing no damage, indicating that the landslide is currently dormant. The shear surface of the landslide is not located in the clays of the Aalbeke Member, but in the more recent smectite-rich Asse clay of the Maldegem Formation.

Frequency–area distribution of landslides

Figure 8 shows the frequency–size distribution $f(A_L)$ of all landslides mapped in the study area. The grey hashed lines are the theoretical density curves produced by Malamud et al. (2004) for landslide inventories with magnitude (M_L) 4 and 5 which corresponds to 10^4 and 10^5 landslides (N_L). These curves show a negative power–law scaling for medium-size and large landslides, and a positive power–law scaling for small landslides. From results obtained by Malamud et al. (2004) for several historical inventories, one might expect for landslides in Flanders a $f(A_L)$ with these two scaling regimes, but with a shift of the rollover towards larger areas since evidence of many of the smaller landslides has been lost. The $f(A_L)$ obtained for landslides in Flanders indeed shows two scaling regimes, but similar to the landslide inventory of the Flemish Ardennes, one of them deviates from the theoretical curves. Instead of a positive and negative power–law relation for small and medium-size to large landslides respectively, $f(A_L)$ consists of two negative power–law relations:

$$f(A_L) = 1104.50A_L^{-0.45} \left(R^2 = 0.94\right) \quad (3)$$

for landslides with $A_L<10^{-2}$ km^2; and

$$f(A_L) = 2.39A_L^{-1.88} \left(R^2 = 0.98\right) \quad (4)$$

for landslides with $A_L\geq10^{-2}$ km^2.

Eq. (4) was also calculated without inclusion of the Alden Biesen DGSD. This resulted in a relation with a slightly higher power–law exponent:

$$f(A_L) = 1.85A_L^{-1.96} \left(R^2 = 0.98\right) \quad (5)$$

Topographical threshold

A significant negative power–law relation was observed between the average landslide slope and upstream drainage area ($R^2=0.04$; $Pr>F=0.0016$; $n=234$; Fig. 9). From this relation the topographical threshold for deep-seated landslides in the study area was derived as:

$$S = 0.084\ A^{-0.055} \left(R^2 = 0.04\right) \quad (6)$$

The two DGSDs are indicated as outliers in the graph and were not taken into account for the calculation of this threshold. Especially the Alden Biesen landslide plots well below the threshold line.

Landslide susceptibility

As illustrated in Table 2 the six classes of the intermediate susceptibility map were further combined to obtain the final landslide

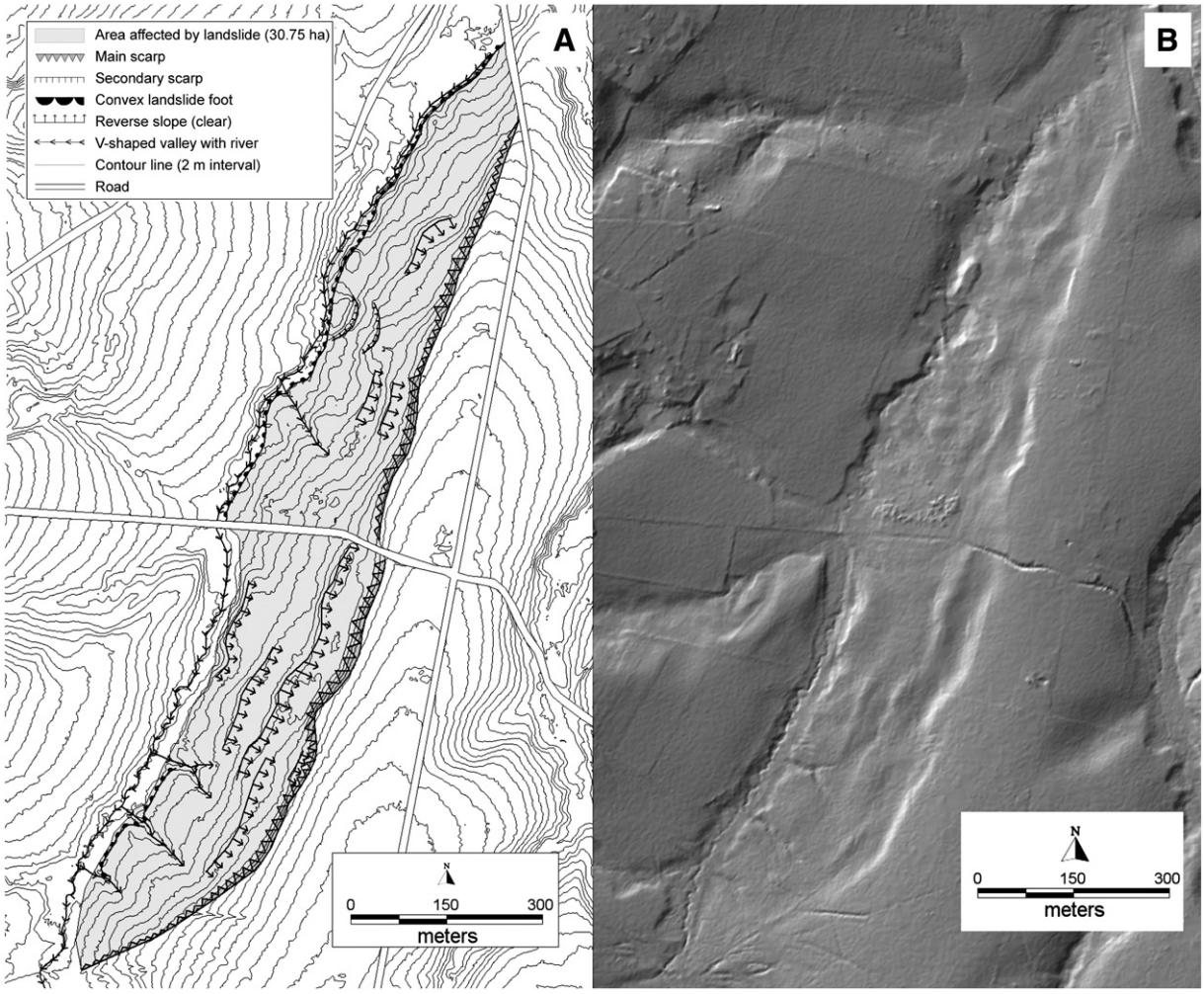

Figure 6. The Hallerbos landslide near Dworp, a representative deep-seated rotational slide ($A_L = 30.75$ ha; see nr. 2 in Fig. 1F). (A) Geomorphological map. (B) Excerpt of the LiDAR-derived shaded-relief map. Note that this landslide has a width/length $\gg 1$.

susceptibility map (Fig. 10) showing areas with high or low susceptibility. All areas with high landslide susceptibility have a clayey lithology and a minimum S of 8%. This slope threshold was chosen because mapped landslides generally have $S \geq 8\%$ (Fig. 9). As mapped landslides occupy 0.28% of the study area, it is not appropriate to consider a large proportion of the study area as susceptible. Therefore, the final landslide susceptibility map classifies only 4% of Southern Flanders as susceptible to landsliding. Sixty-four percent of the landslide-affected areas are located within this susceptible area. This might seem a rather small percentage, but as stated before, we focus on predicting the landslide depletion areas and these were generally very well predicted by the model.

Discussion

Use of LiDAR

This study used LiDAR-derived shaded-relief maps, expert knowledge and field checks to generate a landslide inventory for a large region. It shows that landslides in Southern Flanders are more widespread than previously thought, as more than 330 old and recent landslides were identified in five hilly regions (Fig. 1). However, verification of LiDAR-derived landslide inventories is required to exclude human-disrupted hillslope sections incorrectly indicated as presumed landslides.

Dissimilar $f(A_L)$ curve and S-A graph

In contrast to $f(A_L)$ published for many landslide distributions, the $f(A_L)$ distribution for Southern Flanders consists of two negative power–law relations (Eq. 3 and 4). The relation found for medium-size to large landslides has an exponent of 1.88. This is within the range of -2.3 ± 0.6 derived from a literature review by Van Den Eeckhaut et al. (2007b). For large landslides the decrease in frequency with increasing A_L could be related to the decrease in possible locations where large landslides still can occur. Mapped shallow landslides in Flanders occurred almost all within the last 50 years and were often at least partly caused by local human activities decreasing local slope stability. Their affected area is relatively small because of the generally low local response to small interventions. Similar to Van Den Eeckhaut et al. (2007b) we suggest that the model of Malamud et al. (2004: grey hashed lines in Fig. 8) is mainly valid for mountain regions where the surface morphology and lithology are the result of tectonic uplift and erosion and weathering processes, making a large fraction of the area marginally stable, and where landslides are triggered by a natural triggering factor such as rainfall, earthquake shaking or rapid snowmelt or by an anthropogenic intervention with regional impact (e.g. widespread deforestation). More recently, ten Brink et al. (2009) also suggested this hypothesis. Southern Flanders, on the other hand, is a densely populated hilly region located relatively far from plate boundaries where Holocene tectonic activity is relatively low, though not completely absent. The decrease of recent

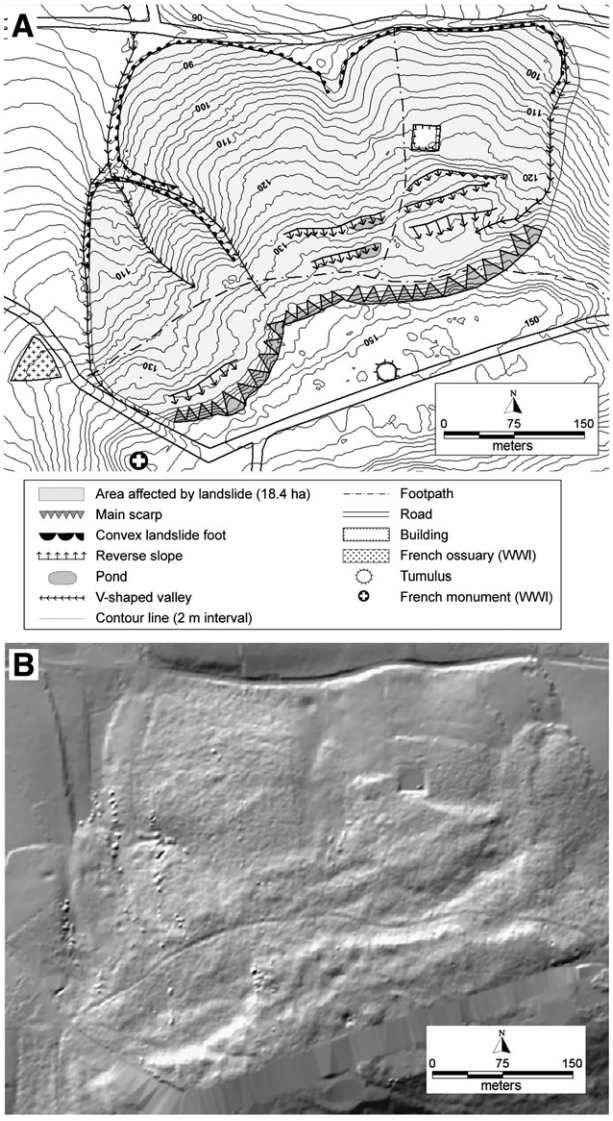

Figure 7. The Kemmelberg landslide near Kemmel, a representative deep-seated rotational slide (A_L = 18.4 ha; see nr. 1 in Fig. 1D). (A) Geomorphological map. (B) Excerpt of the LiDAR-derived shaded-relief map.

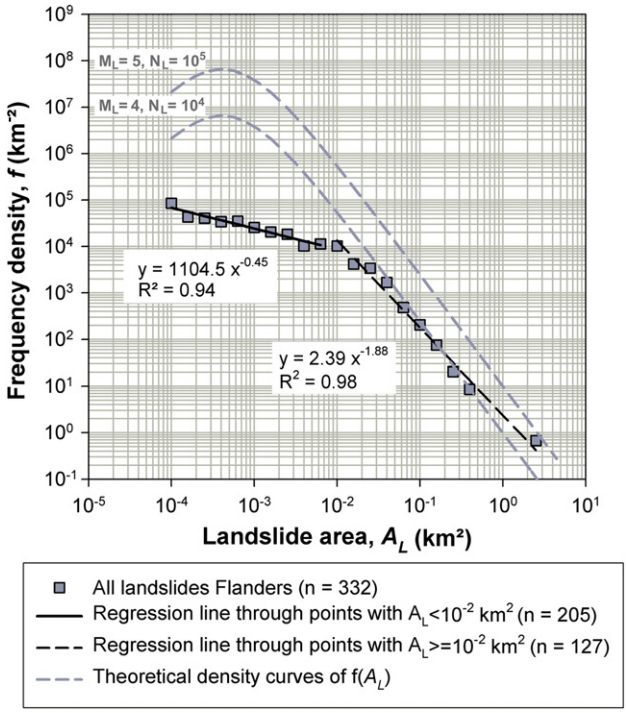

Figure 8. Dependence of landslide frequency density, f, on landslide area, A_L, for the landslide inventory in Southern Flanders. Grey hatched lines represent landslide frequency distributions corresponding to the general landslide probability distribution proposed by Malamud et al. (2004) for landslide inventories with magnitude (M_L) 4 and 5 which corresponds to 10^4 and 10^5 landslides (N_L).

small landslides with landslide size following a negative power–law with a relatively low exponent might be related to the fact that in the populated hilly study area recent landslides are only rarely caused by a natural trigger alone, and that local human interventions contribute to local landslide initiation or reactivation with limited spatial impact. The observation that the f(A_L) of old, large landslides is similar to f(A_L) found in mountain regions suggests that the large landslides were caused by natural factors under environmental conditions that differ from the current conditions of low intensity rainfall events and relatively low tectonic activity.

We also investigated the topographical thresholds of the landslides in Southern Flanders. Montgomery and Dietrich (1994a) define all slopes with S below 40% as unconditionally stable, i.e. stable even when saturated. They plotted data for North America and found a change in process dominance from slopes mainly affected by landslides to slopes mainly affected by processes dominated by overland flow (Fig. 9). Landslide initiation points typically had S above 50% and small A, and gully initiation points had lower S but larger A, the latter resulting in higher values for the area coefficient b. The same relation between S and A was found for landslides in Rwanda (Moeyersons, 2003) and hydrologically triggered landslides in Congo (Moeyersons et al., 2004). The topographical threshold obtained for the deep-seated landslides in Southern Flanders is significantly lower than those for North America (1994b; Fig. 9), Rwanda and Congo, and the

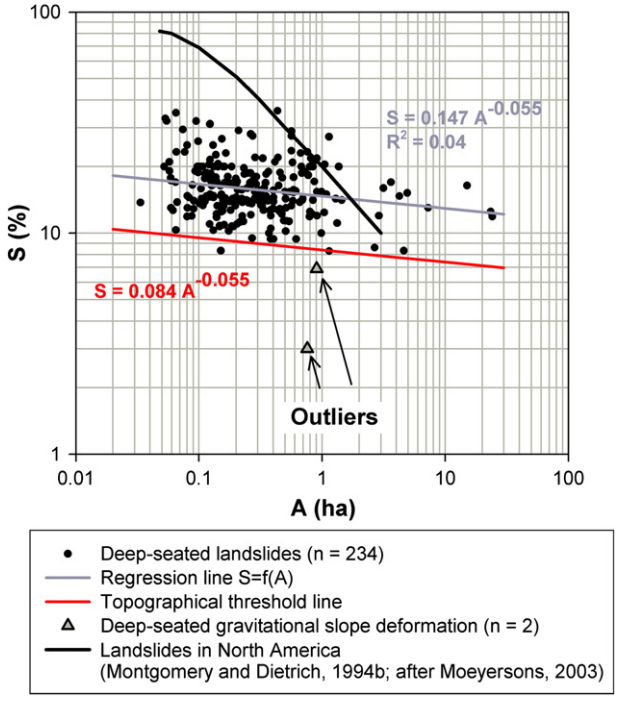

Figure 9. Relation between drainage area (A) versus soil surface slope (S) and indication of the topographical threshold for Holocene deep-seated landslides in Southern Flanders and shallow landslides in North America. For Flanders, both S and A are calculated from a LiDAR-derived DTM. The two outliers are the two DGSDs observed in this study.

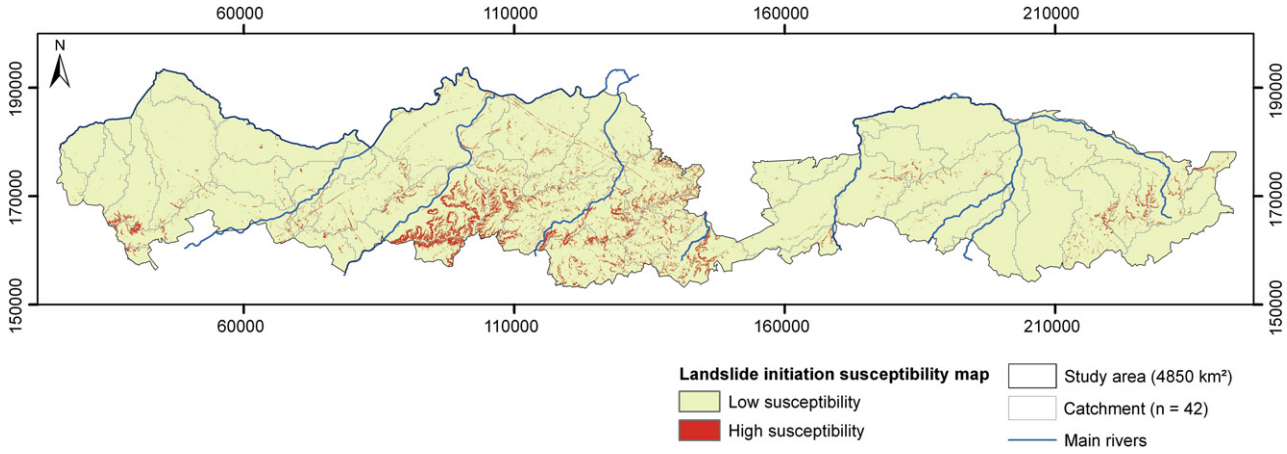

Figure 10. Landslide susceptibility map of Southern Flanders as derived from an heuristic model using slope gradient and lithology (Table 3) as independent factors controlling landslide occurrence (Belgian Lambert 72 coordinates; m).

low value of b (−0.055; Eq. 6) indicates that A is of minor importance for landslide initiation in Southern Flanders. Whatever the A-value is, the lower threshold for S is always between 8 and 10%.

Hypotheses for the initiation of deep-seated landslides in southern Flanders

Currently, little is known about the age and triggering factors of the deep-seated landslides in Southern Flanders. Only one study in the Flemish Ardennes (Van Den Eeckhaut et al., 2007c) attempted to unravel the age and history of an old landslide in Flanders. With AMS radiocarbon dating of organic material found at the bottom of ponds located in reverse slopes, the Collinabos landslide was dated 8700–8440 cal yr BP. This date corresponds with the end of the Boreal (8700–7800 BP) and suggests an initiation or important reactivation during the early Holocene, a relatively wet period coinciding with permafrost melting, and is in agreement with conditions reported for landsliding in low-gradient regions of France (Champagne region; Guérémy and Vejux, 1987) and Ukraine (Pánek et al., 2008). Probably other landslides were initiated in Flanders during this period, but the subdued topography of some landslides, especially of the DGSDs hypothesizes that some landslides are pre-Holocene.

Apart from a climatic trigger, some old deep-seated landslides might also be related to faults present in the study area. Faults can contribute to landsliding in different ways. Seismic activity along active faults can trigger landslides (e.g. Keefer, 1984, 1994; Rodríguez et al., 1999), but fault zones can also be weaker zones along which landslides preferentially occur (Sosson et al., 2009). With regard to seismic activity as a possible trigger of historical landslides Crozier (1992) (in Jibson, 1996) listed six criteria supporting a seismic trigger. These are (1) the large size of the landslides; (2) the ongoing seismicity in the region; (3) the coincidence of the landslide locations with active faults; (4) a landslide distribution that can not be explained solely on the basis of geological or geomorphological conditions; (5) the presence of liquefaction features; and (6) geotechnical slope stability analyses showing the requirement of earthquake shaking for inducing the landslides. For the Flemish Ardennes Ost et al. (2003) found that the first, second and fourth criteria were met. However, they did not investigate the location of the faults. Figure 1 shows faults and historical earthquakes related to the Nieuwpoort Asquemont Fault Zone and to the Roer Graben. For both fault zones earthquakes with magnitudes around 6 are possible. A link between quaternary activity of the Roer Graben and the occurrence of old landslides in the Pays de Herve (Southeast Belgium) was already suggested by Demoulin et al. (2003). Hence, also the third criterion is met. The fifth and the sixth criteria are still not investigated, but it is unlikely that stability models predict slope failure under wet conditions alone.

From our results we can suggest two other indications favouring a relation between the landslide and fault locations. First, the two DGSDs are outliers in the S-A graph (Fig. 9). Moeyersons et al. (2004) reported four landslides in Congo with S-A values significantly different from the values of the other landslides. While the other landslides were located in a tectonically stable region and were believed to be mainly triggered by a hydrological factor, these four landslides were located along a tectonically active fault. The authors concluded that tectonically triggered landslides plot lower in S-A graphs. If this explanation is true, then the lower location of the DGSDs (and perhaps other landslides in the study area) in the S-A graph suggests the possibility of a link between these landslides and the fault locations.

A second indication for a fault-related origin was derived from a further analysis of the landslide susceptibility map. For this, the study area was subdivided in 42 subcatchments (Fig. 10) using WATEM/SEDEM and for each subcatchment both the proportion of landslide-affected and landslide susceptible areas were calculated. Figure 11 shows the graph plotting these two variables. The hypothesis is that if all landslides in Southern Flanders have the same triggering factor, then regions with a high spatial occurrence of landslide susceptible areas should indeed be affected by many landslides and vice versa. In other words, these data for all subcatchments are then expected to plot close to the regression line. One catchment in Haspengouw, the one containing the two DGSDs, and two catchments in the Flemish Ardennes deviate from the other catchments because they have a high percentage of landslide-affected areas compared to the percentage classified as susceptible by the model. These regions contain more landslides than expected which might be attributed to the occurrence of a local landslide trigger, such as an earthquake along one of the active faults in the immediate neighbourhood. On the other hand, most catchments in the West Flemish hills, the Flemish Ardennes, Hageland and western Haspengouw plot close to the regression line. Especially Hageland and western Haspengouw are located relatively far from faults. With the exception of the catchment in which the Hallerbos landslides are located, a higher percentage of landslide-affected areas would be expected in the catchments in Pajottenland. The lower spatial occurrence of landslides might be due to the absence of a major local landslide trigger. To conclude, it can be stated that both climatic and seismic conditions during the Quaternary may have caused landslides in Southern Flanders. Indications favouring a link between the faults, either as earthquake triggers or as weaker zones, and landslides have been identified. However, one of the most

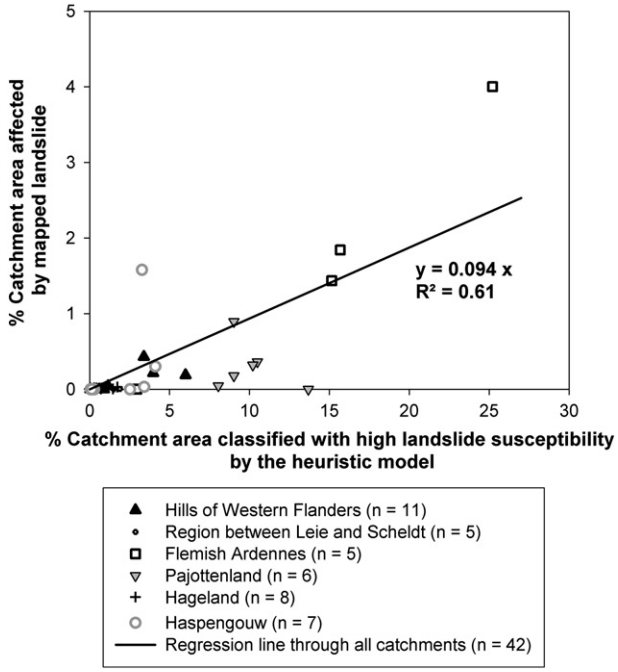

Figure 11. Percentage of the catchment area affected by landslides versus percentage of the catchment area classified with high landslide susceptibility for 42 subcatchments in Southern Flanders. See Fig. 10 for the location of the subcatchments and Figure 1A for the regions in Flanders.

important indications, the existence of a historical document linking landslide activity to an earthquake has not been found.

Conclusions

Analysis of LiDAR-derived shaded-relief maps and field checks allowed generation of a landslide inventory for Southern Flanders (4850 km^2). This study revealed that landslides are more widespread than previously thought, as more than 330 old deep-seated rotational earth slides, complex earth slides, DGSDs and recent, shallow complex earth slides were identified. In the study area the highest landslide density occurs west of Brussels where hilly regions with clay lithology are more abundant (Figs. 1 and 10). Although east of Brussels only 37 landslides were mapped, some of them, especially the Alden Biesen DGSD, affected a considerable area. Investigation of the morphological and topographical characteristics of the landslides revealed differences compared to well-accepted landslide characteristics observed in steeper terrain. First of all, the S-A threshold line (Fig. 9) plots well below threshold lines obtained for other landslide inventories and shows that landslide initiation is mainly depending on slope gradient with a lower threshold between 8 and 10%. This lower slope threshold and the presence of clays and marls were selected for the development of a scoring matrix, and the landslide susceptibility map (Fig. 10) was successful in predicting zones where landslides have been initiated. Secondly, also f(A_L) deviates from the so-called theoretical density curves (Fig. 8). Similar to earlier results obtained for the 205 landslides in the Flemish Ardennes (Van Den Eeckhaut et al., 2007b) two negative power–law relations were obtained. The negative relation for medium-size to large landslides is probably related to morphological characteristics of the study area. The negative relation for the recent, small landslides, however, might be related to the limited spatial impact of most anthropogenically triggered landslides in the study area. Although further analysis of the initiation conditions for the deep-seated landslides is needed, several indications suggest a relation between active faults and some of the landslides. Also the age of the landslides needs further investigation, because AMS radiocarbon dating is only available for one landslide. These dates suggest an initiation or reactivation during the end of the Boreal period, but the subdued morphology of other landslides suggests a pre-Holocene age. It can be concluded that landslides occurring on low-gradient residual hills are more important in landscape evolution of hilly areas in Europe developed on loose Tertiary sediments than was hitherto thought and that LiDAR can effectively contribute to their identification.

Acknowledgments

Before joining JRC, the first author received grant-aided support from the Research Foundation-Flanders (FWO), Belgium. Roland Dreesen is thanked for providing information on an interesting outcrop within the Alden Biesen landslide. Thanks go also to the two anonymous referees and the editors for their critical comments which helped to improve this paper.

References

AGIV, 2001. Tertiary geological map of Belgium, Agentschap voor Geografische Informatie Vlaanderen, Gent, Belgium, Digital file.
AGIV, 2005. LIDAR hoogtepunten – brondata van Digitaal Hoogtemodel Vlaanderen, MVG-LIN-AMINAL-afdeling Water en MVG-LIN-AWZ-afdeling Waterbouwkundig Laboratorium en Hydrologisch onderzoek, Brussel, Belgium, Digital file.
Ardizzone, F., Cardinali, M., Galli, M., Guzzetti, F., Reichenbach, P., 2007. Identification and mapping of recent rainfall-induced landslides using elevation data collected by airborne Lidar. Natural Hazards and Earth System Sciences 7, 637–650.
Booth, A.M., Roering, J.J., Perron, J.T., 2009. Automated landslide mapping using spectral analysis and high-resolution topographic data: Puget Sound lowlands, Washington, and Portland Hills, Oregon. Geomorphology 109, 132–147.
Buffel, P., Matthijs, J., 2009. Toelichtingen bij de geologische kaart van België: Vlaams Gewest, Kaartblad 31–39 Brussel-Nijvel, 1:50,000. Ministerie van de Vlaamse Gemeenschap Afdeling Natuurlijke Rijkdommen en Energie, Brussel, Belgium.
Camelbeeck, T., 1997. The study of active faults in stable continental Europe: examples in the Roer Graben and in the Belgian seismic active zone. Aardkundige Mededelingen 8, 35–38.
Camelbeeck, T., Alexandre, P., Vanneste, K., Meghraoui, M., 2000. Long-term seismicity in regions of present day low seismic activity: the example of western Europe. Soil Dynamics and Earthquake Engineering 20, 405–414.
Chacksfield, B.C., De Vos, W., D'Hooghe, L., Dusar, M., Lee, M.K., Poitevin, C., Royles, C.P., Verniers, J., 1993. A new look at Belgian aeromagnetic and gravity data through image-based display and integrated modelling techniques. Geological Magazine 130, 583–591.
Claes, S., Frederickx, E., Gullentops, F., 2001. Toelichtingen bij de geologische kaart van België: Vlaams Gewest, Kaartblad 34 Tongeren, 1:50, 000. Ministerie van de Vlaamse Gemeenschap Afdeling Natuurlijke Rijkdommen en Energie, Brussel, Belgium.
Cruden, D.M., Varnes, D.J., 1996. Landslide types and processes. In: Turner, A.K., Schuster, R.L. (Eds.), Landslides, Investigation and Mitigation, Transportation Research Board. National Research Council, Special Report 247. National Academy Press, Washington, DC, pp. 36–71.
Debacker, T.N., Herbosch, A., Verniers, J., Sintubin, M., 2004. Faults in the Asquempont area, southern Brabant Massif, Belgium. Netherlands Journal of Geosciences 83, 49–65.
De Keersmaeker, L., Baeté, H., Christiaens, B., Esprit, M., Van de Kerckhove, P., Vandekerkhove, K., 2007. Bosreservaat Jansheideberg (Hallerbos): Monitoringrapport; monitoring van de dendrometrische gegevens en de vegetatie in de steekproefcirkels en de kernvlakte. Instituut voor Natuur- en Bosonderzoek, Geraardsbergen, Belgium.
Demoulin, A., Pissart, A., Schroeder, C., 2003. On the origin of late Quaternary palaeolandslides in the Liège (E Belgium) area. International Journal of Earth Sciences 92, 795–805.
De Vos, W., Verniers, J., Herbosch, A., Vanguestaine, M., 1993. A new geological map of the Brabant Massif, Belgium. Geological Magazine 130, 606–611.
Dewitte, O., Chung, C.J., Demoulin, A., 2006. Reactivation hazard mapping for ancient landslides in West Belgium. Natural Hazards and Earth System Sciences 6, 653–662.
Dreesen, R., Dusar, M., Matthijs, J., Van Den Eeckhaut, M., Gullentops, F., Poesen, J., in press. An exceptionally well-preserved landslide tongue near Alden Biesen (Province of Limburg): the relevance of temporary exposures of the subsoil for elucidating complex geological history. In: Meylemans, E., De Bie, M., Cordemans, K., Poesen, J., Van Peer, Ph., Verstraeten, G. (Eds.), The Archaeology of Erosion, the Erosion of Archaeology, Proceedings of the Brussels Conference, 28–30 April 2008, Relicta Monografieën. Archeologie, Monumenten- en Landschapsonderzoek in Vlaanderen/Heritage Research in Flanders, Brussels.
Dunning, S.A., Mitchell, W.A., Petley, D.N., Rosser, N.J., Cox, N.J., 2007. Landslides predating and triggered by the 2005 Kashmir earthquake: rockfall to rock avalanches. Geophysical Research Abstracts 9, 06376.
Ercanoğlu, M., 2003. Production of landslide susceptibility maps using fuzzy log and statistical methods: West Black Sea region (South of Kumlace – North of Yenice), Geological Engineering Dept. Hacettepe University, Ph.D. thesis, pp. 203.
GIS-Vlaanderen, 2003. Nieuwsbrief GIS-Vlaanderen: Digitaal Hoogtemodel Vlaanderen. Ondersteunend Centrum GIS-Vlaanderen, Gent, Belgium.
Glenn, N.F., Streutker, D.R., Chadwick, D.J., Thackray, G.D., Dorsch, S.J., 2006. Analysis of LiDAR-derived topographic information for characterizing and differentiating landslide morphology and activity. Geomorphology 73, 131–148.

Guérémy, P., Vejux, V., 1987. Mouvements de terrains successifs: les glissements et les coulées du versant sud de la Montagne d'Avize (Marne-France). Travaux de l'Institut de Géographie de Reims 69–72, 113–127.
Gullentops, F., Claes, S., 1997. The Bilzen fault bundle (NE Belgium). Aardkundige Mededelingen 8, 99–102.
Guthrie, R.H., Evans, S.G., 2004. Analysis of landslide frequencies and characteristics in a natural system, coastal British Columbia. Earth Surface Processes and Landforms 29, 1321–1339.
Halet, F., 1904. Glissements de terrain aux environs de Renaix. Bulletin de la Société Belge de Géologie 18, 161–163.
Haneberg, W.C., 2005. The Ins and Outs of Airborne LIDAR: an introduction for practicing engineering geologists. AEG news 48, 16–19.
Haneberg, W.C., Cole, W.F., Kasali, G., 2009. High-resolution lidar-based landslide hazard mapping and modeling, UCSF Parnassus Campus, San Francisco. USA Bulletin of Engineering Geology and the Environment 68, 263–276.
Haugerud, R.A., Harding, D.J., Johnson, S.Y., Harless, J.L., Weaver, C.S., Sherrod, B.L., 2003. High resolution Lidar topography of the Puget Lowland, Washington—a bonanza for earth science. GSA Today 13, 9.
Issler, D., De Blasio, F.V., Elverhoi, A., Bryn, P., Lien, R., 2005. Scaling behaviour of clayrich submarine debris flows. Marine and Petroleum Geology 22, 187–194.
Jacobs, P., De Ceukelaire, M., De Breuck, W., De Moor, G., 1999. Toelichting bij de geologische kaart van België: Vlaams gewest, kaartblad 29 Kortrijk, schaal 1/50, 000. Ministerie van Economische zaken en Ministerie van de Vlaamse Gemeenschap, Brussel.
Jenniskens, A., 1989. Nieuwen Biesen in Alden Biesen: 5 eeuwen Duitse Orde in Maastricht. Bilzen-Maastricht, Netherlands.
Jibson, R.W., 1996. Use of landslides for paleoseismic analysis. Engineering Geology 43, 291–323.
Kasai, M., Ikeda, M., Asahina, T., Fujisawa, K., 2009. LiDAR-derived DEM evaluation of deep-seated landslides in a steep and rocky region of Japan. Geomorphology 113, 57–69.
Keaton, J.R., DeGraff, J.V., 1996. Surface observation and geologic mapping. In: Turner, A.K., Schuster, R.L. (Eds.), Landslides: Investigation and Mitigation, Transportation Research Board. National Research Council. National Academy Press, Washington, DC, pp. 128–230.
Keefer, D.K., 1984. Landslides caused by earthquakes. Geological Society of American Bulletin 95, 406–421.
Keefer, D.K., 1994. The importance of earthquake-induced landslides to long-term slope erosion and slope-failure hazards in seismically active regions. Geomorphology 10, 265–284.
Korup, O., Clague, J.J., 2009. Natural hazards, extreme events, and mountain topography. Quaternary Science Reviews 28, 977–990.
Lefèvre, M.A., 1926–1927. Glissements de terrain dans les collines de Renaix. Annales de la Société géologique de Belgique 50, 29–35.
Malamud, B.D., Turcotte, D.L., Guzzetti, F., Reichenbach, P., 2004. Landslide inventories and their statistical properties. Earth Surface Processes and Landforms 29, 687–711.
Mather, A.E., Griffiths, J.S., Stokes, M., 2003. Anatomy of a fossil landslide from the Pleistocene of SE Spain. Geomorphology 50, 135–149.
McKean, J., Roering, J., 2004. Objective landslide detection and surface morphology mapping using high-resolution airborne laser altimetry. Geomorphology 47, 331–351.
Moeyersons, J., 2003. The topographic thresholds of hillslope incisions in southwestern Rwanda. Catena 50, 381–400.
Moeyersons, J., Tréfois, Ph., Lavreau, J., Alimasi, D., Badriyo, I., Mitima, B., Mundala, M., Munganga, D., Nahimana, L., 2004. A geomorphological assessment of landslide origin at Bukavu, Democratic Republic of the Congo. Engineering Geology 72, 73–87.
Montgomery, D.R., 1994. Road surface drainage, channel initiation and slope instability. Water Resources Research 30, 1925–1932.
Montgomery, D.R., Dietrich, W.E., 1994a. A physically based model for the topographic control on shallow landsliding. Water Resources Research 30, 1153–1171.
Montgomery, D.R., Dietrich, W.E., 1994b. Landscape dissection and drainage area–slope threshold. In: Kirkby, M.J. (Ed.), Process Models and Theoretical Geomorphology. John Wiley and Sons Ltd, Chichester, pp. 221–246.
Moro, M., Saroli, M., Tolomei, C., Salvi, S., 2009. Insights on the kinematics of deep-seated gravitational slope deformations along the 1915 Avezzano earthquake fault (Central Italy), from time-series DInSAR. Geomorphology 112, 261–276.
Ost, L., Van Den Eeckhaut, M., Poesen, J., Vanmaercke-Gottigny, M.C., 2003. Characteristics and spatial distribution of large landslides in the Flemish Ardennes. Zeitschrift für Geomorphologie N.F. 47, 329–350.
Pánek, T., Hradecký, J., Smolková, V., Šilhán, K., 2008. Gigantic low-gradient landslides in the northern periphery of the Crimean Mountains (Ukraine). Geomorphology 95, 449–473.
Poesen, J., Nachtergaele, J., Verstraeten, G., Valentin, C., 2003. Gully erosion and environmental change: importance and research needs. Catena 50, 91–133.
Rodríguez, C.E., Bommer, J.J., Chandler, R.J., 1999. Earthquake-induced landslides: 1980–1997. Soil Dynamics and Earthquake Engineering 18, 325–346.
Rowlands, K.A., Jones, L.D., Whitworth, M., 2003. Landslide Laser Scanning: a new look at an old problem. Quarterly Journal of Engineering Geology and Hydrogeology 36, 155–157.
Schulz, W.H., 2007. Landslide susceptibility revealed by LIDAR imagery and historical records, Seattle, Washington. Engineering Geology 89, 67–87.
Siddle, R., C., Pearce, A.J., O'Loughin, C.L., 1985. Hillslope stability and land use. American Geophysical Union, Water Resources Monograph 11, Washington, D.C.
Somville, O., 1939. De Belgische Aardbeving van 11 Juni 1938. Drukkerij J. Duculot, Gembloux, Belgium.
Sosson, C., Devos, A., Lejeune, O., Marre, A., 2009. Contribution to the study of underground quarries: the underground quarry at Glennes (Aisne - France). Acte du 4th International Symposium on Archaeological Miming History. Reishelsheim - Odenwald, Germany, pp. 14–25.
Stark, C.P., Hovius, N., 2001. The characterisation of landslide size distributions. Geophysical Research Letters 28, 1091–1094.
Tarolli, P., Tarboton, D.G., 2006. A new method for determination of most likely landslide initiation points and the evaluation of digital terrain model scale in terrain stability mapping. Hydrology and Earth System Sciences 10, 663–677.
ten Brink, U.S., Barkan, R., Andrews, B.D., Chayton, J.D., 2009. Size distributions and failure initiation of submarine and subaerial landslides. Earth and Planetary Science Letters 287, 31–42.
Van Den Eeckhaut, M., Poesen, J., Verstraeten, G., Vanacker, V., Moeyersons, J., Nyssen, J., Van Beek, L.P.H., 2005. The effectiveness of hillshade maps and expert knowledge in mapping old deep-seated landslides. Geomorphology 67, 351–363.
Van Den Eeckhaut, M., Vanwalleghem, T., Poesen, J., Govers, G., Verstraeten, G., Vandekerckhove, L., 2006. Prediction of landslide susceptibility using rare events logistic regression: a case-study in the Flemish Ardennes (Belgium). Geomorphology 76, 392–410.
Van Den Eeckhaut, M., Poesen, J., Verstraeten, G., Vanacker, V., Nyssen, J., Moeyersons, J., Van Beek, L.P.H., Vandekerckhove, L., 2007a. The use of LIDAR-derived images for mapping old landslides under forest. Earth Surface Processes and Landforms 32, 754–769.
Van Den Eeckhaut, M., Poesen, J., Govers, G., Verstraeten, G., Demoulin, A., 2007b. Characteristics of the size distribution of recent and historical landslides in a populated hilly region. Earth and Planetary Science Letters 256, 588–603.
Van Den Eeckhaut, M., Verstraeten, G., Poesen, J., 2007c. Morphology, and internal structure of a dormant landslide in a hilly area: the Collinabos landslide (Belgium). Geomorphology 89, 258–273.
Van Doorselaer, A., Putman, R., Van der Gucht, K., Janssens, F., 1987. De Kemmelberg, een Keltische bergvesting. Westvlaamse Archaeologica. Monografieën III, Kortrijk, Belgium.
Vanmaercke-Gottigny, M., 1980. Landslides as a morphogenetic phenomenon in a hilly region of Flanders (Belgium). In: De Boodt, M., Gabriels, D. (Eds.), Assessment of Erosion. John Wiley and Sons, Chichester, pp. 475–484.
Vanwalleghem, T., Poesen, J., Nachtergaele, J., Verstraeten, G., 2005. Characteristics, controlling factors and importance of deep gullies under cropland on loess-derived soils. Geomorphology 69, 76–91.
Van Westen, C.J., 1993. Application of geographical information system to landslide hazard zonation. ITC publication no 15, ITC, Enschede, Netherlands.
Verachtert, E., Van Den Eeckhaut, M., Poesen, J., Deckers, J., 2010. Factors controlling the spatial distribution of soil piping erosion on loess-derived soils: a case study from Central-Belgium. Geomorphology 119, 339–348.
Verstraeten, G., Van Oost, K., Van Rompaey, A., Poesen, J., Govers, G., 2002. Evaluating an integrated approach to catchment management to reduce soil loss and sediment pollution through modelling. Soil Use and Management 18, 386–394.